

A COMPARISON BETWEEN SPATIAL INTERPOLATION APPROACHES IN A HEAD-TRACKED ACTIVE HEADREST SYSTEM

Chung Kwan Lai*

Jordan Cheer

Institute of Sound and Vibration Research (ISVR) University of Southampton, United Kingdom.

ABSTRACT

The integration of head-tracking can improve the achievable performance of active noise control headrest systems by allowing the mismatch between the plant model used by the controller and the physical plant response to be reduced. Although previous studies have shown that the performance improvement achieved through head-tracking is limited by the resolution of the tracking system, this limitation can be addressed by either interpolating between plant models obtained at different head positions and then calculating the required controller, or interpolating between a set of pre-computed controllers optimised for different head positions. The differences in performance between the two approaches to interpolation, however, have not been explored, despite various interpolation strategies being previously utilised in head-tracked active control systems discussed in the literature. This paper presents a comparison between the two approaches to spatial interpolation for a head-tracked active headrest system. Assuming a tonal disturbance, it is shown through numerical simulations that the performance benefit brought by spatial interpolation differs between the two approaches to interpolation.

Keywords: active headrest system, local active noise control, head-tracker, interpolation

1. INTRODUCTION

The use of active noise control to provide local control of sound at a listener's ears dates back to the 1950s [1], how-

*Corresponding author: C.K.Lai@soton.ac.uk.

Copyright: ©2025 Lai et al. This is an open-access article distributed under the terms of the Creative Commons Attribution 3.0 Unported License, which permits unrestricted use, distribution, and reproduction in any medium, provided the original author and source are credited.

ever, it has recently attracted renewed interest due to the potential for integrating head-tracking techniques to extend the bandwidth of effective control [2]. In the context of an active headrest system [3], where secondary loudspeakers are typically placed near the headrest, a headtracker can be used to detect the current position of the user's head and update either the plant model, which is then used to compute the controller, or the precomputed controller itself, both of which would be obtained during a calibration stage. In either case, this updating process can reduce the mismatch between the physical and assumed responses for the physical head position, thereby improving control performance in response to head movements. While it is ideal for the head-tracker and corresponding system updates to be as accurate as possible to maximise the control performance, such an approach may not be feasible in practice, as this would require a lengthy calibration process to measure the plant responses and optimal controllers for many head positions. Previous research has been conducted to determine how the tracking accuracy influences the performance and stability of an active headrest system and ultimately to define the required tracking accuracy for a given level and bandwidth of performance [4,5]. However, rather than utilising an extremely fine tracking resolution, an alternative approach is to interpolate between the responses [6] for a coarser tracking resolution to improve their accuracy. Although it seems relatively straightforward that the performance of the active headrest system will depend on the accuracy provided by the interpolation algorithm used, there are in fact two approaches to interpolation: in the first case, the plant responses corresponding to the coarse measurement grid are interpolated directly and the optimal controller is then calculated using the interpolated plant responses; in the second case, the interpolation is instead performed between the optimal controllers calculated for each head position







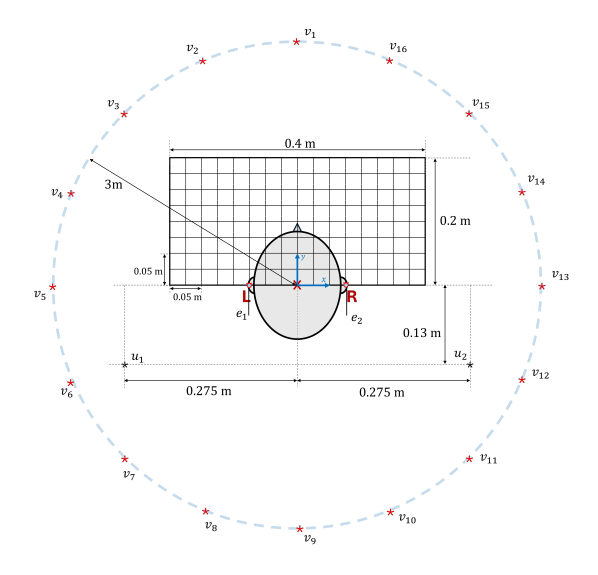


Figure 1: Configuration for the active headrest where the head translates in the sway (left/right) and surge (front/back) direction within a $(0.4~\text{m}\times0.2~\text{m})$ translational grid. The minimum grid spacing for the translational grid is 0.025~m.

on the coarse measurement grid. This paper presents a comparison between the control performance for the two proposed approaches to interpolation applied to an active headrest system. Sec. 2 describes the active headrest and introduces the two spatial interpolation approaches; Sec. 3 describes the interpolation algorithm used to realise the interpolation in both cases; Sec. 4 presents the results from the simulation study; and conclusions are drawn in Sec. 5.

2. FORMULATION OF ACTIVE HEADREST CONTROL PROBLEM

Fig. 1 illustrates the numerically simulated configuration of the active headrest, which employs a boundary element model of the KU100 head [7] implemented in COMSOL to represent the user's head. Two monopole point sources, driven by control signals u_1 and u_2 , simulate the secondary sources in the active headrest; whilst the disturbance sound field is generated by 16 incoherent primary sources, driven by the complex source strengths $v_1 - v_{16}$, positioned around the head, as depicted in Fig. 1. The feedforward control strategy used to minimise the signals at the user's ears is shown in Fig. 2, where each diagram illustrates a different interpolation approach for updating

the control filter, **W**, based on the current location of the head. Assuming that the disturbance signal is tonal, the cost function that aims to minimise the error signals located at the user's ears can be expressed in the frequency domain, as

$$J = \mathbb{E} \left[\mathbf{e}^{H} \mathbf{e} + \beta \mathbf{u}^{H} \mathbf{u} \right]$$
$$= \operatorname{tr} \left\{ \mathbb{E} \left[\mathbf{e} \mathbf{e}^{H} + \beta \mathbf{u} \mathbf{u}^{H} \right] \right\}$$
(1)

where e and u denote complex vectors of the error signals and control signals, respectively, and $\beta=0$ is the regularization parameter. Based on the block diagram shown in Fig. 2, the complex vector of error signals is given by

$$e = d + Gu = d + GWx,$$
 (2)

where **W** and **G** are matrices of control filters and the physical plant responses, respectively, and **x** is the complex vector of reference signals. Assuming that the physical plant responses are perfectly known, the optimal control filter matrix can therefore be derived as [8]

$$\mathbf{W}_{opt} = -\left[\mathbf{G}^{\mathrm{H}}\mathbf{G} + \beta \mathbf{I}\right]^{-1}\mathbf{G}^{\mathrm{H}}\mathbf{S}_{xd}\mathbf{S}_{xx}^{-1}, \quad (3)$$

where \mathbf{S}_{xd} is the spectral density matrix between the disturbance and reference signals, and $\mathbf{S}_{xx} = \mathbf{I}$ is the spectral density matrix of the reference signals, following the general notation $\mathbf{S}_{xy} = \mathbb{E}\left[\mathbf{y}\mathbf{x}^{\mathrm{H}}\right]$.

During the initial calibration phase, the plant responses were directly obtained for a subset of head positions within a discrete translational grid of $(0.4 \text{ m} \times 0.2 \text{ m})$, marked by the red crosses in Fig. 3. The corresponding optimal control filters for these head positions were then calculated using Eqn. (3). The use of a coarser resolution reflects the practical constraints encountered on calibration complexity and duration. For the remaining grid points, the control filter can be determined utilising the two different approaches to interpolation, as outlined in Fig. 2. In the controller-based interpolation approach, as shown in Fig. 2a, the control filter is calculated by directly interpolating between the optimal control filters computed for the head positions included in the calibration process, and the interpolated control filter is denoted as \mathbf{W} . In contrast, in the plant-based interpolation strategy, as shown in Fig. 2b, the plant model and spectral density at the target head position are first estimated by interpolating between the responses measured in the calibration, and then the control filters are calculated using the interpolated responses, as

$$\mathbf{W}_{o} = -\left[\mathbf{G}^{\mathrm{H}}\mathbf{G} + \beta \mathbf{I}\right]^{-1}\mathbf{G}^{\mathrm{H}}\mathbf{S}_{xd}\mathbf{S}_{xx}^{-1},\tag{4}$$







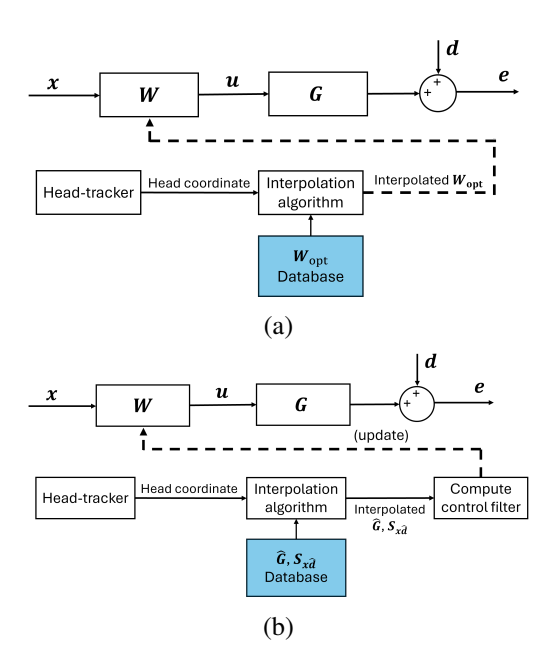


Figure 2: The multichannel feedforward control system used in the head-tracker equipped active headrest system, featuring (a): controller-based interpolation and (b): plant-based interpolation architecture.

where \mathbf{G} and \mathbf{S}_{xd} denote the interpolated plant model and spectral density matrices respectively.

To compare the performance of the two approaches to interpolation, the control performance of the active headrest system at the interpolated grid points can be assessed by computing the attenuation performance at the i-th error microphone, given by

$$L_{e,i} = -10\log_{10} \left| \frac{\mathbf{S}_{e_i e_i}}{\mathbf{S}_{d_i d_i}} \right|. \tag{5}$$

3. SPATIAL INTERPOLATION BASED ON KERNEL RIDGE REGRESSION

While various interpolation algorithms are available, to compare the two approaches to interpolation described in the previous section, the Kernel-ridge interpolation method will be utilised. This algorithm has recently been applied to sound-field estimation and a spatial active noise control system [9, 10], and is described in this section.

Consider a general complex matrix $\mathbf{H}(\psi) \in \mathbb{C}^{(I \times J)}$, where ψ represents the vector of head coordinates, and

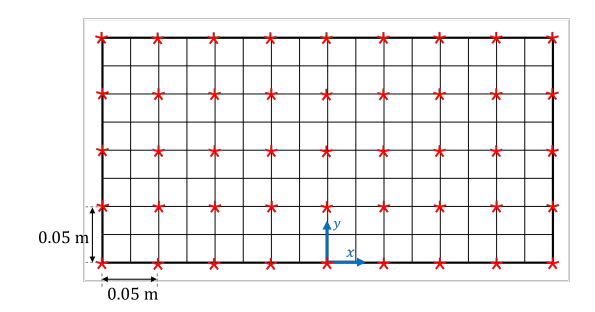


Figure 3: Head positions within the translational grid, marked by red crosses, indicate locations where plant responses were directly measured during the calibration phase.

the element at the i-th row and j-th column is denoted by $h_{ij}(\psi)$. In this context, **H** may represent either the control filter W, plant model G, or spectral density S_{xd} , depending on the interpolation approach being utilised. During the calibration phase, the matrix is measured at discrete grid positions, which are denoted as $\mathbf{H}(\psi_n)$ for the nth position. The goal of interpolation is to estimate each element of **H** at an arbitrary position ψ using the corresponding elements from the pre-measured matrices $\hat{\mathbf{H}}$ at the known positions ψ_n . Each element of $\overset{\cdot}{\mathbf{H}}$ can be calculated according to the interpolation function given as $h_{ij}(\psi) = \phi^{\mathrm{H}}(\psi)\mathbf{f}$, where $\phi(\psi)$ is the input feature vector that is a function of head coordinates ψ , and f is the complex weighting vector containing the coefficients that determine the contribution of each feature vector components. The cost function, which minimises the sum of squared errors between the interpolated and pre-measured elements across all discrete head positions, is defined as

$$J_{ij} = \sum_{n=1}^{N} \left| \underline{h}_{ij}(\boldsymbol{\psi}_n) - \hat{h}_{ij}(\boldsymbol{\psi}_n) \right|^2 + \lambda \mathbf{f}^{\mathrm{H}} \mathbf{f}$$
$$= \left(\mathbf{\Phi} \mathbf{f} - \hat{\mathbf{h}}_{ij} \right)^{\mathrm{H}} \left(\mathbf{\Phi} \mathbf{f} - \hat{\mathbf{h}}_{ij} \right) + \lambda \mathbf{f}^{\mathrm{H}} \mathbf{f}, \qquad (6)$$

where N is the total number of discrete grid points used during the calibration phase, and

$$\mathbf{\Phi} = \left[\boldsymbol{\phi}^{\mathrm{H}}(\boldsymbol{\psi}_1) \; \boldsymbol{\phi}^{\mathrm{H}}(\boldsymbol{\psi}_2) \; \cdots \; \boldsymbol{\phi}^{\mathrm{H}}(\boldsymbol{\psi}_N) \right]^{\mathrm{T}}, \quad (7)$$

$$\hat{\mathbf{h}}_{ij} = \left[\hat{h}_{ij}(\boldsymbol{\psi}_1) \; \hat{h}_{ij}(\boldsymbol{\psi}_2) \; \cdots \; \hat{h}_{ij}(\boldsymbol{\psi}_N) \right]^{\mathrm{T}}, \quad (8)$$

are the generic input feature matrix and the vector of premeasured elements across all grid points, respectively, and







 λ is the regularisation factor. The optimal ${\bf f}$ is therefore given as

$$\mathbf{f}_{opt} = \left[\mathbf{\Phi}^{\mathrm{H}} \mathbf{\Phi} + \lambda \mathbf{I} \right]^{-1} \mathbf{\Phi}^{\mathrm{H}} \hat{\mathbf{h}}_{ij}. \tag{9}$$

However, the value of \mathbf{f}_{opt} depends on the choice of Φ , which may involve a much higher number of dimensions than the number of grid points. Instead, the cost function can be kernelized to overcome the dimensionality curse imposed by the generic input feature vector [11]. By letting $\mathbf{f} = \Phi^{\mathrm{H}} \alpha$, where α is the intermediate complex variable vector, the cost function from Eqn. (6) can be expressed in terms of α to give

$$J_{ij} = \boldsymbol{\alpha}^{\mathrm{H}} \left[(\mathbf{K}\mathbf{K} + \lambda \mathbf{K}) \right] \boldsymbol{\alpha} - \boldsymbol{\alpha}^{\mathrm{H}} \mathbf{K} \hat{\mathbf{h}}_{ij} - \hat{\mathbf{h}}_{ij}^{\mathrm{H}} \mathbf{K} \boldsymbol{\alpha} + \hat{\mathbf{h}}_{ij}^{\mathrm{H}} \hat{\mathbf{h}}_{ij},$$
(10)

where $\mathbf{K} = \mathbf{\Phi}\mathbf{\Phi}^{H}$ is the Gram matrix, which is Hermitian and semi-positive-definite i.e. $\mathbf{K} = \mathbf{K}^{H}$, given by

$$\mathbf{K} = \begin{bmatrix} \kappa(\psi_1, \psi_1) & \kappa(\psi_1, \psi_2) & \cdots & \kappa(\psi_1, \psi_N) \\ \kappa(\psi_2, \psi_1) & \kappa(\psi_2, \psi_2) & \cdots & \kappa(\psi_3, \psi_N) \\ \vdots & \vdots & \ddots & \vdots \\ \kappa(\psi_N, \psi_1) & \kappa(\psi_N, \psi_2) & \cdots & \kappa(\psi_N, \psi_N) \end{bmatrix},$$
(11)

and $\kappa(\psi_m,\psi_n)=\phi^{\rm H}(\psi_m)\phi(\psi_n)$ is denoted as a kernel function. The optimal value of α that minimises Eqn. (10) can then be obtained as

$$\alpha_{opt} = (\mathbf{K} + \lambda \mathbf{I})^{-1} \,\hat{\mathbf{h}}_{ij}. \tag{12}$$

Finally, the interpolated element at an arbitrary position ψ can then be evaluated as

$$h_{ij}(\psi) = \kappa(\psi) \left(\mathbf{K} + \lambda \mathbf{I}\right)^{-1} \hat{\mathbf{h}}_{ij}, \tag{13}$$

where

$$\boldsymbol{\kappa}(\boldsymbol{\psi}) = [\kappa(\boldsymbol{\psi}, \boldsymbol{\psi}_1) \ \kappa(\boldsymbol{\psi}, \boldsymbol{\psi}_2) \ \cdots \ \kappa(\boldsymbol{\psi}, \boldsymbol{\psi}_N)]$$
 (14)

is known as the reproducing Kernel vector.

To gain a preliminary understanding of how different kernel functions affect the controller's performance, two different kernel functions have been used here for interpolation. The first, derived from previous work [10], is constrained by the 3D Helmholtz equation and is given by

$$\kappa(\boldsymbol{\psi}_{m}, \boldsymbol{\psi}_{n}) = \operatorname{sinc}(k||\boldsymbol{\psi}_{m} - \boldsymbol{\psi}_{n}||_{2})$$

$$= \frac{\sin(k||\boldsymbol{\psi}_{m} - \boldsymbol{\psi}_{n}||_{2})}{k||\boldsymbol{\psi}_{m} - \boldsymbol{\psi}_{n}||_{2}}, \quad (15)$$

where $k = \omega/c_0$ is the acoustic wavenumber, and $||\cdot||_2$ denotes the l_2 -norm. The second kernel function, adapted from [12], is a Gaussian kernel scaled according to the wavenumber, defined as

$$\kappa(\boldsymbol{\psi}_m, \boldsymbol{\psi}_n) = \exp\left(-k^2||\boldsymbol{\psi}_m - \boldsymbol{\psi}_n||_2^2\right). \tag{16}$$

To evaluate the accuracy of the interpolation, the overall interpolation error between the interpolated matrix $\widetilde{\mathbf{H}}$ and the true matrix \mathbf{H} at the interpolated head position $\widetilde{\psi}$ is defined as

$$L_{\mathbf{H}}(\psi) = 10 \log_{10} \left| \frac{\sum_{i,j} |h_{ij}(\psi) - \underline{h}_{ij}(\psi)|^2}{\sum_{i,j} |h_{ij}(\psi)|^2} \right|. \quad (17)$$

4. COMPARISON BETWEEN SPATIAL INTERPOLATION APPROACHES

This section evaluates the interpolation accuracy for the interpolation algorithm introduced in Sec. 3 and the performance of the active headrest system is then presented in Sec. 4.2, with a comparison between the two interpolation approaches described in Sec. 2.

4.1 Interpolation accuracy

Fig. 4 and Fig. 5 present the overall interpolation error, calculated according to Eqn. (17), for the G, S_{xd} , and W matrices at all head positions requiring interpolation, corresponding to the unmarked grid points in Fig. 3. To improve the conditioning of the Gram matrix inversion in Eqn. (11), the regularisation parameter for all cases was set to $\lambda = 1 \times 10^{-6}$. When the Helmholtz kernel function from Eqn. (15) is used to interpolate the G and \mathbf{S}_{xd} matrices, the interpolation error, shown in Fig. 4a, remains below -30 dB across all frequencies. Notably, the error for S_{xd} is significantly lower than that for G at all frequencies, highlighting how interpolation accuracy varies between different matrices. In contrast, when using the Gaussian kernel function from Eqn. (16), as shown in Fig. 4b, the estimation error increases with frequency, exceeding -20 dB at some head positions around 900 Hz. This difference arises from the nature of the kernel function itself, as discussed in [10], where the Helmholtz kernel function is better suited for the interpolation of responses that are physically related to the acoustic sound field, such as the acoustic response. While both the plant G and spectral density S_{xd} correspond to the secondary and primary acoustic responses, respectively, the differences in interpolation accuracy between the two may arise







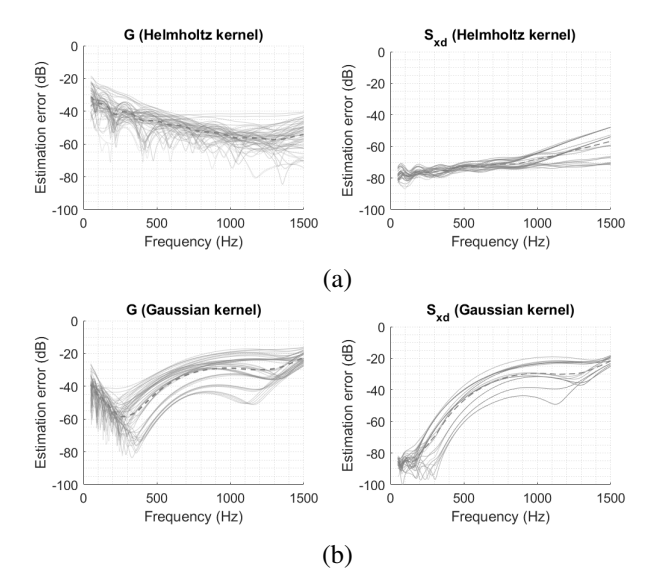


Figure 4: The overall interpolation error, evaluated using Eqn. (17), for the G and S_{xd} matrices as a function of frequency at head positions requiring interpolation. Solid lines represent errors for all head positions requiring interpolation using the (a) Helmholtz kernel from Eqn. (15) and the (b) Gaussian kernel from Eqn. (16), while the dotted line indicates the average interpolation error.

from the fact that the head scattering effect varies more spatially in the near-field compared to the far-field. When both the Helmholtz and Gaussian kernel functions are used to interpolate the control filter, the overall interpolation error, as shown in Fig. 5, is significantly lower compared to that of G and S_{xd} , and increases with frequency. Even though the control filter is directly related to the plant responses, as shown in Eqn. (3), the individual elements of the controller matrix result from the interaction between all elements of the plant due to the matrix inverse and multiplication operation, which results in a lower interpolation accuracy. These results offer valuable insights into how the performance of the active headrest system varies between the spatial interpolation approaches, as further discussed in Sec. 4.2.

4.2 Control performance comparison between spatial interpolation approaches

Fig. 6 and Fig. 7 present the attenuation performance plots for the left error microphone as a function of frequency

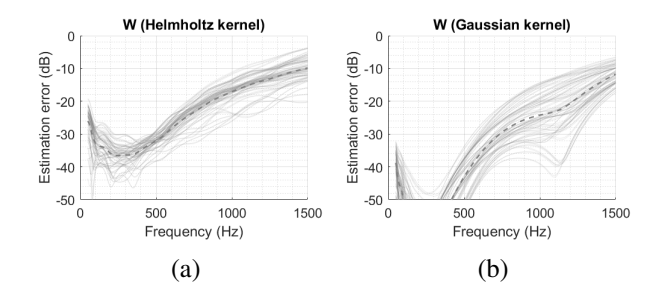


Figure 5: The overall interpolation error, evaluated using Eqn. (17), for the control filter **W** as a function of frequency at head positions requiring interpolation. Solid lines represent errors for all head positions requiring interpolation using the (a) Helmholtz kernel from Eqn. (15) and the (b) Gaussian kernel from Eqn. (16), while the dotted line indicates the average interpolation error.

for all head positions requiring interpolation. Depending on the interpolation approach being applied, interpolation is performed on either the plant responses or precomputed controllers obtained from the marked grid points in Fig. 3. When the controller-based interpolation strategy using the Kernel function from Eqn. (15) is applied (Fig. 6a), the attenuation performance generally decreases with increasing frequency, with less than 10 dB performance being achieved for some head positions at around 900 Hz. In contrast, the attenuation performance is significantly improved when the plant-based interpolation strategy (Fig. 6b) is used, with attenuation levels in excess of 20 dB being achieved across all frequencies. This is likely due to the differences in interpolation accuracy between the plant and controller matrices, as discussed in Sec. 4.1, which results in an upper-frequency limit beyond which the performance achieved by interpolating the controller is limited. When the Gaussian kernel from Eqn. (16) is used in the interpolation algorithm, the performance of both interpolation approaches degrades with increasing frequency. The results for the controller-based approach (Fig. 7a) show a slight improvement compared to those obtained using the Helmholtz kernel function (Fig. 6a) for some head positions. Although the plant-based interpolation approach still performs better than the controllerbased interpolation approach, the results still highlight the importance of selecting the appropriate kernel function when performing spatial interpolation.







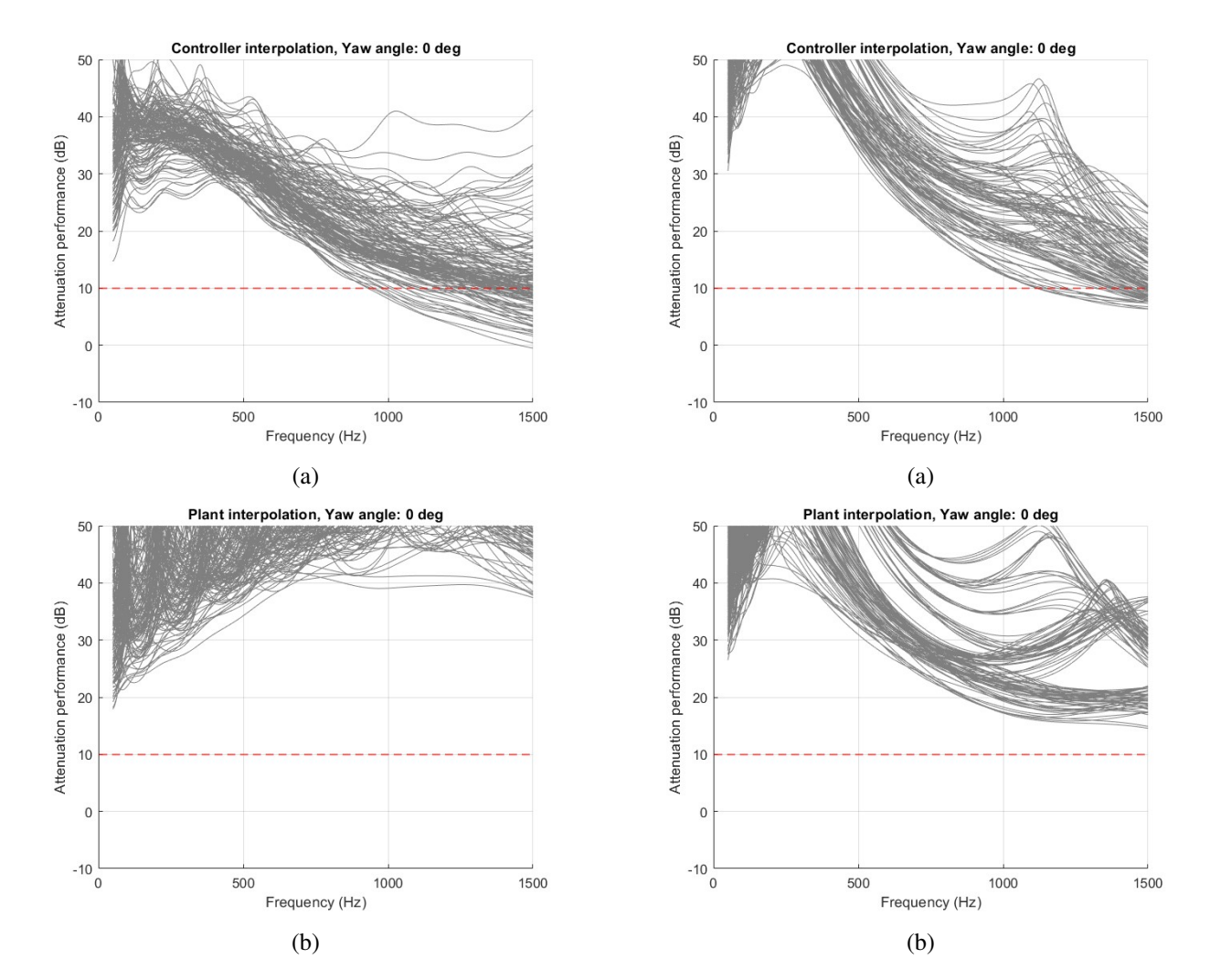


Figure 6: Attenuation performance plots for the left error microphone as a function of frequency for head positions requiring interpolation using the Helmholtz kernel function given by Eqn. (15), shown for (a) the controller-based and (b) the plant-based interpolation method.

Figure 7: Attenuation performance plots for the left error microphone as a function of frequency for head positions requiring interpolation using the gaussian kernel function given by Eqn. (16), shown for (a) the controller-based and (b) the plant-based interpolation method.







5. CONCLUSIONS

Although integrating head-tracking techniques into active noise control headrest systems has been shown to significant enhance control performance, the performance remains constrained by the resolution of head-tracking, which is limited by the calibration procedure. This limitation can be addressed by applying spatial interpolation techniques to estimate the either the controller or the plant responses at head positions that have not been explicitly calibrated. However, the effectiveness of interpolation depends on both the chosen interpolation approach and the utilised interpolation algorithm. This paper has presented two interpolation approaches: one that interpolates between plant models obtained at different head positions before computing the corresponding controller, and another that interpolates directly between a set of precomputed optimal controllers. In both cases the kernel ridge interpolation algorithm has been utilised with different kernel functions being explored. The results from numerical simulations of an active headrest system with head-tracking have demonstrated that when utilising the kernel ridge interpolation algorithm, a significant improvement in control performance is achieved when utilising the plant-based interpolation approach. It has also been shown that the kernel function has a significant impact on the achieved performance, with the Helmholtz kernel function providing a significant performance advantage when utilised with the plant-model interpolation approach, but providing somewhat inferior performance when applied to the controller-based interpolation approach.

6. ACKNOWLEDGMENTS

The work was supported by the project IN-NOVA: Active reduction of noise transmitted into and from enclosures through encapsulated structures, which has received funding from the European Union's Horizon Europe programme under the Marie Sklodowska-Curie grant agreement no. 101073037. This work was funded by UK Research and Innovation under the UK government's Horizon Europe funding guarantee [grant number EP/X027767/1]. Jordan Cheer was supported by the Department of Science, Innovation and Technology (DSIT) Royal Academy of Engineering under the Research Chairs and Senior Research Fellowships programme.

7. REFERENCES

- [1] H. F. Olson and E. G. May, "Electronic Sound Absorber," *The Journal of the Acoustical Society of America*, vol. 25, pp. 1130–1136, Nov. 1953.
- [2] S. J. Elliott, W. Jung, and J. Cheer, "Head tracking extends local active control of broadband sound to higher frequencies," *Scientific Reports*, vol. 8, pp. 1–7, Dec. 2018.
- [3] B. Rafaely, S. J. Elliott, and J. Garcia-Bonito, "Broadband performance of an active headrest," *The Journal of the Acoustical Society of America*, vol. 106, pp. 787–793, Aug. 1999.
- [4] C. K. Lai, J. Cheer, and C. Shi, "The effect of head-tracking resolution on the stability and performance of a local active noise control headrest system," *The Journal of the Acoustical Society of America*, vol. 157, pp. 766–777, Feb. 2025.
- [5] H. Jiang, H. Chen, J. Tao, H. Zou, and X. Qiu, "Accuracy requirements of ear-positioning for active control of road noise in a car," *Applied Acoustics*, vol. 225, p. 110164, Nov. 2024. Read_Status: Done Read_Status_Date: 2024-11-11T22:45:18.126Z.
- [6] J. Y. Oh, H. W. Jung, M. H. Lee, K. H. Lee, and Y. J. Kang, "Enhancing active noise control of road noise using deep neural network to update secondary path estimate in real time," *Mechanical Systems and Signal Processing*, vol. 206, p. 110940, Jan. 2024. Read_Status: Done Read_Status_Date: 2024-10-16T20:57:28.691Z.
- [7] F. Di Giusto, S. Van Ophem, W. Desmet, and E. Deckers, "Analysis of laser scanning and photogrammetric scanning accuracy on the numerical determination of Head-Related Transfer Functions of a dummy head," *Acta Acustica*, vol. 7, p. 53, 2023.
- [8] S. Elliott, Signal Processing for Active Control. Academic Press, 2000.
- [9] S. Koyama, J. Brunnstrom, H. Ito, N. Ueno, and H. Saruwatari, "Spatial Active Noise Control Based on Kernel Interpolation of Sound Field," *IEEE/ACM Transactions on Audio, Speech, and Language Pro*cessing, vol. 29, pp. 3052–3063, 2021. Read_Status: Done Read_Status_Date: 2024-09-22T08:31:58.734Z.
- [10] S. Koyama, J. G. C. Ribeiro, T. Nakamura, N. Ueno, and M. Pezzoli, "Physics-Informed Machine Learning for Sound Field Estimation: Fundamentals, state







of the art, and challenges [Special Issue On Model-Based and Data-Driven Audio Signal Processing]," *IEEE Signal Processing Magazine*, vol. 41, pp. 60–71, Nov. 2024.

- [11] N. Cristianini and J. Shawe-Taylor, *An introduction to support vector machines: And other kernel-based learning methods*. Cambridge: Cambridge University Press, 2013. OCLC: 1031088649.
- [12] N. Ueno, S. Koyama, and H. Saruwatari, "Kernel Ridge Regression with Constraint of Helmholtz Equation for Sound Field Interpolation," in 2018 16th International Workshop on Acoustic Signal Enhancement (IWAENC), (Tokyo), pp. 1–440, IEEE, Sept. 2018.



